Vapor−Liquid Equilibrium in Electric Field Gradients

Sela Samin and Yoav Tsori*

Department of Chemical Engineering and The Ilse Katz Institute for Nanoscale Science and Technology, Ben-Gurion University of the Negev, 84105 Beer-Sheva, Israel

Received: August 10, 2010; Revised Manuscript Received: November 11, 2010

We investigate the vapor−liquid coexistence of polar and nonpolar fluids in the presence of a nonuniform electric field. We find that a large enough electric field can nucleate a gas bubble from the liquid phase or a liquid droplet from the vapor phase. The surface tension of the vapor−liquid interface is determined within squared-gradient theory. When the surface potential (charge) is controlled, the surface tension increases (decreases) compared to the zero-field interface. The effect of the electric field on the fluid phase diagram depends strongly on the constitutive relation for the dielectric constant. Finally, we show that gas bubbles can be nucleated far from the bounding surfaces.

1. Introduction

The phase behavior of fluids in external electric fields has drawn increasing interest in recent years. Theoretical[1−5] and experimental[6−8] investigations thus far focused mainly on the application of a uniform field. The first treatment of dielectric fluids in uniform electric fields was that of Landau and Lifshitz.[1] Their mean-field results predicted a small change in the fluid's critical temperature ΔT_c. For typical fields used in experiments ($\cong 10^7$ V/m) ΔT_c is rather small, of the order of milliKelvins. Dipolar fluids, with more complex phase behavior due to the dipole−dipole interaction, have been studied more recently.[2−5] Simulations of Stockmayer fluids found reasonable agreement with mean-field theory.[5] Experiments in pure fluids and low molecular weight binary mixtures agree with the theory on the magnitude of ΔT_c, but reports in the literature on the sign of the change are conflicting.[8−11] The effect of a uniform gravitational field on vapor−liquid coexistence is even smaller and can only be detected very close to fluid's critical point.[12]

Field gradients naturally occur in complex systems like microfluidic devices and colloidal suspensions. In nonpolar binary mixtures, nonuniform electric fields, originating from the proximity to a curved charged object, can induce a phase-separation transition and change the phase diagram substantially.[13−15] In polar binary mixtures, the existence of salt leads to intrinsically nonuniform fields. Here, a small amount of ions can modify the phase equilibrium and surface tension of the mixture considerably.[16−19]

Here we show, on the mean-field level, that the effect of nonuniform fields on the vapor−liquid coexistence can be quite large. For concreteness we use a simple van der Waals theory together with Onsager's theory of dielectrics to treat fluids placed in condensers at constant voltage or charge. The paper is organized as follows: In section 2 the van der Waals theory is extended to include the contribution of electric fields. In section 3.1 we describe the field-induced phase transition and calculate the density and pressure profiles. In section 3.2 we explore the field effect on the temperature−density phase plane in various circumstances. In section 3.3 we use gradient theory to calculate the surface tension change due to the electric field. In section 3.4 we give an example of a complex electrode configuration: the quadrupolar electrode array. In this configuration we demonstrate that phase separation can occur away from the confining surfaces. Conclusions are given in section 4.

2. Model

We consider a one-component van der Waals fluid. We characterize the fluid by its temperature T and density $\rho = N/V$, where N is the number of molecules and V the volume. In the presence of an external field the density is allowed to change in space and the Helmholtz free energy is expressed as

$$F = \int [f_{vdw}(T,\rho) + f_{es}(T,\rho,\mathbf{r})]\mathrm{d}\mathbf{r} \quad (1)$$

where f_{es} is the electrostatic energy density and f_{vdw} is the van der Waals free energy density given by[20]

$$f_{vdw} = k_B T\rho[\log(\rho\Lambda^3) - 1 - \log(1 - \rho b)] - a\rho^2 \quad (2)$$

Here, Λ is the thermal de Broglie wavelength and k_B is the Boltzmann constant. The parameter b accounts for the reduction in effective volume due to the hard-core repulsion; $b = (2\pi d^3)/3$, where d is the molecular hard-core diameter. The parameter a takes into account the pairwise attractive interaction between the fluid molecules. Within the mean-field approximation a is given by

$$a = -\frac{1}{2}\int_d^\infty u(r)\mathrm{d}\mathbf{r} \quad (3)$$

where $u(r)$ is the spherically symmetric interaction potential between a pair of molecules. The modified Lennard−Jones potential with hard-core repulsion is a natural choice for the van der Waals fluid

* To whom correspondence should be addressed: E-mail: tsori@bgu.ac.il.

10.1021/jp107529n
Published on Web 12/10/2010

$$u(r) = \begin{cases} \infty & r < d \\ -\Delta r^{-6} & r > d \end{cases} \quad (4)$$

where Δ is a constant. Putting eq 4 in eq 3 we have $a = 2\pi\Delta/(3d^3)$. In the absence of an electric field, the fluid's pressure P is given by $P = \rho(\partial f_{vdw}/\partial\rho) - f_{vdw}$ and hence the van der Waals equation of state is $(P + a\rho^2)(1 - b\rho) = \rho k_B T$.

The fluid's equilibrium density is obtained by minimization of F under the constraint that the total number of molecules is conserved. Thus, one needs to minimize the functional $\Omega = \int \omega \, d\mathbf{r}$, where

$$\omega = f - \mu\rho \quad (5)$$

is the grand potential density. The Lagrange multiplier μ is identified as the chemical potential. The van der Waals theory predicts qualitatively correct the first-order vapor−liquid phase transition. Below the critical temperature T_c, the integrand in eq 5 has two minima corresponding to vapor and liquid phases with densities $\rho_v(T)$ and $\rho_l(T)$, respectively. Coexisting equilibrium phases appear at a chemical potential $\mu = \mu_c$ determined by the Maxwell construction. This corresponds to the two phases having the same grand potential density $\omega(\rho,T)$. The locus of densities $\rho_{l,v}(T)$ gives the fluid's phase diagram in the temperature−density plane. The densities $\rho_v(T)$ and $\rho_l(T)$ terminate at the critical point $(T_c,\rho_c) = (8a/(27k_B b),(3b)^{-1})$. From the equation of state one finds for the critical pressure $P_c = a/(27b^2)$. In the following we use reduced quantities of density, temperature, and pressure: $\phi = \rho/\rho_c$, $t = T/T_c$, and $p = P/P_c$.

In the presence of an external electric field the fluid is polarized and we add the electrostatic energy density f_{es} to the total energy. We do not include nonlinear polarization effects in f_{es} since they are important only in very large fields ($\gtrsim 10^8$ V/m) at which dielectric breakdown frequently occurs.[21] When the electrostatic potential ψ is prescribed on the bounding surfaces f_{es} is given by[22,23]

$$f_{es}(\rho, \mathbf{E}) = -\frac{1}{2}\varepsilon(\rho)\mathbf{E}^2 \quad (6)$$

where $\mathbf{E} = -\nabla\psi$ is the electric field and ε is the fluid's permittivity. When the total charge Q is prescribed on the bounding surfaces, f_{es} is given by[22,23]

$$f_{es}(\rho, \mathbf{D}) = \frac{1}{2}\frac{\mathbf{D}^2}{\varepsilon(\rho)} \quad (7)$$

where $\mathbf{D}$ is the electric displacement field and we assume the linear relation $\mathbf{D} = \varepsilon\mathbf{E}$ for the isotropic fluid.

In order to correctly describe the fluid on submicrometer scale we employ gradient theory[24] and add a $|\nabla\rho|^2$ term to the free energy, namely,

$$F = \int \left[\frac{1}{2}m|\nabla\rho|^2 + f_{vdw} + f_{es}\right] d\mathbf{r} \quad (8)$$

where the positive parameter m is given by[24,25]

$$m = -\frac{1}{6}\int_d^\infty u(r) r^2 \, d\mathbf{r} \quad (9)$$

From eqs 4 and 9 we obtain $m = 2\pi\Delta/3d = ad^2$.

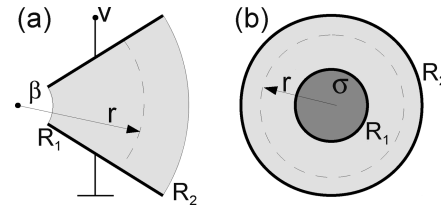

Figure 1. Two model systems. (a) Wedge condenser made of two flat electrodes with a potential difference V across them and an angle β between them. r is the distance from the imaginary meeting point of the electrodes. R_1 and R_2 are radii of the electrode's edge. (b) Charged cylindrical wire with radius R_1 or condenser made of two concentric cylinders with radii R_1 and R_2. The inner cylinder surface charge density is σ.

Extremization of the free energy with respect to ρ and ψ gives the Euler−Lagrange equations[18,19,25,26]

$$\frac{\delta\Omega}{\delta\rho} = -m\nabla^2\rho + \frac{\delta f_{vdw}}{\delta\rho} - \frac{1}{2}\frac{d\varepsilon(\rho)}{d\rho}(\nabla\psi)^2 - \mu = 0 \quad (10)$$

$$\frac{\delta\Omega}{\delta\psi} = \nabla\cdot(\varepsilon(\rho)\nabla\psi) = 0 \quad (11)$$

The constitutive relation $\varepsilon = \varepsilon(\rho)$ couples Gauss's law (eq 11) with eq 10. In the canonical ensemble, μ is an adjustable parameter needed to conserve mass: $\langle\rho\rangle = \rho_0$, where ρ_0 is the average density. An equation similar to eq 10 is obtained for the fluid density in a gravitational field,[12,27] but the coupling of the density to the Laplace equation is unique to electromagnetic fields. We will also treat the grand-canonical ensemble in which the chemical potential is set by the chemical potential μ_0 of the reservoir. On the system boundaries we impose the condition $\mathbf{n}\cdot\nabla\rho = 0$, where $\mathbf{n}$ is the outward unit vector normal to the surface.[28] This boundary condition corresponds physically to a vanishing surface field. In order to elucidate the influence of the electric field, we do not consider any direct short- or long-range interactions between the fluid and the confining solid surfaces.

We begin by considering the two elementary model geometries shown schematically in Figure 1. In these geometries the solution of eqs 10 and 11 is greatly simplified since one can easily calculate the electric field as a function of the density. The first geometry is the cylindrical condenser made up of two concentric cylinders of radii R_1 and R_2. In the limit $R_2 \to \infty$, this reduces to an isolated wire of radius R_1 and surface charge density σ.

In cylindrical symmetry the solution of eq 11 is $\mathbf{E}(r) = \sigma R_1/(\varepsilon(\phi)r)\hat{\mathbf{r}}$, where r is the distance from the inner cylinder's center and σ is the surface charge density. A similar setup has been used by Lee et al., who investigated the phase equilibrium of lipid monolayers.[29] The above expression for $\mathbf{E}$ also applies to a charged spherical colloid with radius R_1; the main difference is that in this case the field decays as r^{-2}. The second geometry we consider is the wedge condenser, made up from two flat electrodes with a potential difference V across them and an angle β between them. Here also, symmetry requires that $\rho = \rho(r)$ and the solution of eq 11 is $\mathbf{E}(r) = (V/\beta r)\hat{\theta}$, where r is the distance from the imaginary meeting point of the electrodes and θ is the azimuthal angle. This and similar designs have been used by Chaikin and co-workers to investigate phase equilibria of colloidal suspensions in electric field gradients.[30−32]

The governing equations are now one dimensional and decoupled, and thus, we are left with the task of solving eq 10 for the van der Waals fluid. We rewrite eq 10 for the cylinders as

$$\tilde{m}\nabla^2\phi = \frac{\partial \tilde{f}_{\mathrm{vdw}}}{\partial \phi} - M_{\mathrm{sc}}\frac{\mathrm{d}\tilde{\varepsilon}/\mathrm{d}\phi}{\tilde{\varepsilon}^2}\tilde{r}^{-2} - \tilde{\mu} \qquad (12)$$

where $\tilde{f}_{\mathrm{vdw}} \equiv f_{\mathrm{vdw}}/P_{\mathrm{c}}$, $\tilde{r} \equiv r/R_1$ is the scaled radius, $\tilde{m} \equiv 3d^2/{R_1}^2$, and $\tilde{\varepsilon} \equiv \varepsilon/\varepsilon_0$ is the dimensionless permittivity (ε_0 is the vacuum permittivity). Here, $M_{\mathrm{sc}} \equiv \sigma^2/(2P_c\varepsilon_0)$ is the dimensionless magnitude of the maximal electrostatic energy density in units of the critical pressure. For the wedge condenser we similarly obtain

$$\tilde{m}\nabla^2\phi = \frac{\partial \tilde{f}_{\mathrm{vdw}}}{\partial \phi} - M_{\mathrm{w}}\frac{\mathrm{d}\tilde{\varepsilon}}{\mathrm{d}\phi}\tilde{r}^{-2} - \tilde{\mu} \qquad (13)$$

where $M_{\mathrm{w}} \equiv \varepsilon_0 V^2/(2P_c\beta^2{R_1}^2)$ is the scaled field squared.

Before we continue we need to specify the nature of the constitutive relation $\tilde{\varepsilon}(\rho)$ of the fluid. For the dielectric constant of a polar fluid Onsager's relation[33] holds

$$\frac{(\tilde{\varepsilon} - \tilde{\varepsilon}_\infty)(2\tilde{\varepsilon} + \tilde{\varepsilon}_\infty)}{\tilde{\varepsilon}} = \left(\frac{\tilde{\varepsilon}_\infty + 2}{3}\right)^2 \frac{{\mu_{\mathrm{D}}}^2}{k_{\mathrm{B}}T\varepsilon_0}\rho \qquad (14)$$

where μ_{D} is the molecular dipole moment and $\tilde{\varepsilon}_\infty$ is the high-frequency limit of the permittivity, as given by the Clausius−Mossotti equation[34]

$$\frac{\tilde{\varepsilon}_\infty - 1}{\tilde{\varepsilon}_\infty + 2} = \frac{\alpha}{3\varepsilon_0}\rho \qquad (15)$$

where α is the molecular polarizability. Equation 14 predicts quite well the dielectric constant of polar materials.[34] However, since it neglects short-range orientational order of the fluid molecules (e.g., hydrogen bonds) it underestimates the dielectric constant in cases where these short-range effects are important. For nonpolar fluids we use Onsager's relation with $\mu_{\mathrm{D}} = 0$, that is, $\tilde{\varepsilon}$ is given by the Clausius−Mossotti equation. Since the van der Waals system is bistable in the absence of electric fields, we expect a phase-separation transition to occur in nonuniform electric fields.[14,15] In the next section we show that this is in fact the case.

3. Results and Discussion

3.1. Phase Separation. Typical equilibrium density profiles $\phi(r)$ obtained from eqs 12 and 13 at a temperature $T < T_{\mathrm{c}}$ in the sharp interface limit ($m = 0$) are presented in Figure 2. For a homogeneous vapor phase in the absence of an electric field, if M is small, a smoothly decaying profile develops (dashed line). The density is higher where the field is strong (small $\tilde{r}$) due to the dielectrophoretic force which favors a higher permittivity (density) fluid in the region of strong field.[14,15]

Above a critical value of M, the dielectrophoretic force nucleates a liquid phase (solid line) with an interface at $\tilde{r} = \tilde{R}$ ($\tilde{R} \simeq 1.3$ in Figure 2a). An increase of M moves the interface to larger radius (dash-dot line, $\tilde{R} \simeq 1.52$ in Figure 2a). The nucleation of a liquid drop from the vapor phase occurs first at $\tilde{R} = \tilde{R}_1$ where the electric field is maximal.

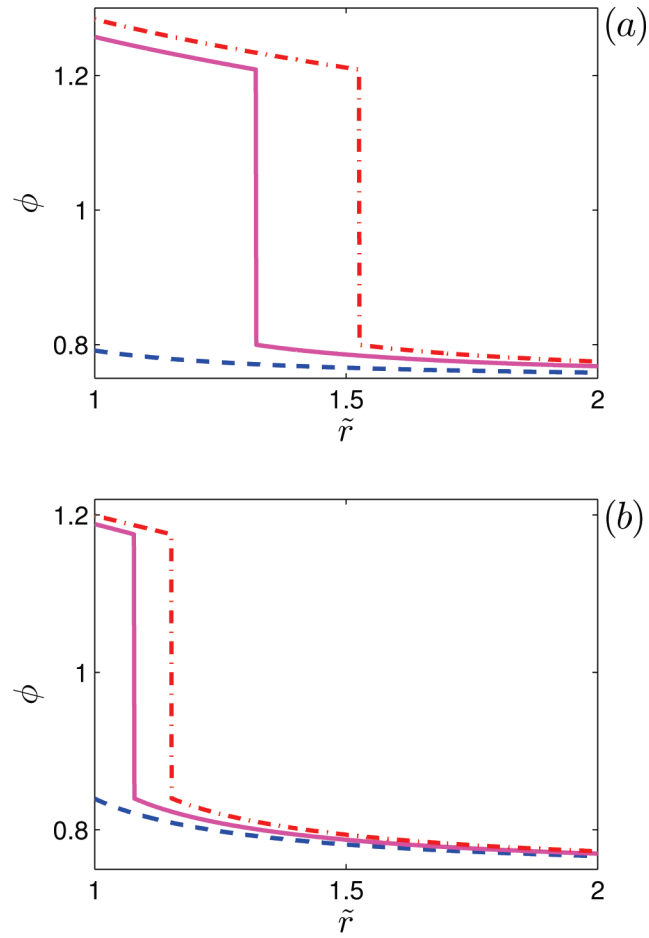

Figure 2. Equilibrium density profiles $\phi(\tilde{r})$ in the sharp interface limit ($m = 0$) at a temperature $t = T/T_{\mathrm{c}} = 0.99$ and a reservoir density $\phi_0 = 0.75$ (vapor phase, $p_0 = 0.952$). (a) Wedge condenser: (dashed line) $M_{\mathrm{w}} = 1.5 \times 10^{-3}$ is smaller than the demixing critical value; (solid line) $M_{\mathrm{w}} = 2 \times 10^{-3}$ is large enough to induce phase separation; (dash-dot line) when M_{w} increases to 4×10^{-3} the interface is at larger radius. (b) The same for a wire with $M_{\mathrm{sc}} = 0.06$ (dashed line), 0.07 (solid line), and 0.08 (dash-dot line). We used the molecular data of acetonitrile ($T_{\mathrm{c}} = 545$ K, $P_{\mathrm{c}} = 4.85$ MPa).[35]

We can estimate the typical demixing charge/voltage from the value of M being in the range $M \approx 0.001-0.1$. Consider a wire of radius 1 μm placed in a vapor of a polar fluid, for example, acetonitrile ($T_{\mathrm{c}} = 545$ K, $P_{\mathrm{c}} = 4.85$ MPa, $d = 5.14$ Å, $\mu_{\mathrm{D}} = 3.93$ D),[35] at $t = 0.99$. Then, the typical demixing electric field is of the order of 10^6-10^7 V/m. This is a large field but still below the dielectric breakdown for many fluids near T_{c}.[21] This field corresponds to a wire voltage of 10−100 V or equivalently to charge densities per unit length of the wire of $10^4 - 10^5$ e charges/μm.

Typical values of M in the wedge condenser are an order of magnitude smaller than in the cylindrical condenser. In the wedge condenser $\mathbf{E}$ is perpendicular to $\nabla\phi$ and hence to the dielectric interface, and therefore, the dielectrophoretic force (proportional to $\mathrm{d}\tilde{\varepsilon}/\mathrm{d}\phi$) exists without the energy penalty proportional to $(\mathrm{d}\tilde{\varepsilon}/\mathrm{d}\phi)^2$ occurring when the dielectric interfaces are parallel to $\mathbf{E}$.[36]

For a fluid dielectric in an external field and in mechanical equilibrium, the fluid's pressure is a tensor P_{ik} which depends on position. In an electric field it is given by[18,22]

$$P_{ik} = \left(\rho\frac{\partial f(\rho,\mathbf{E})}{\partial \rho} - f(\rho,\mathbf{E})\right)\delta_{ik} - E_iD_k \qquad (16)$$

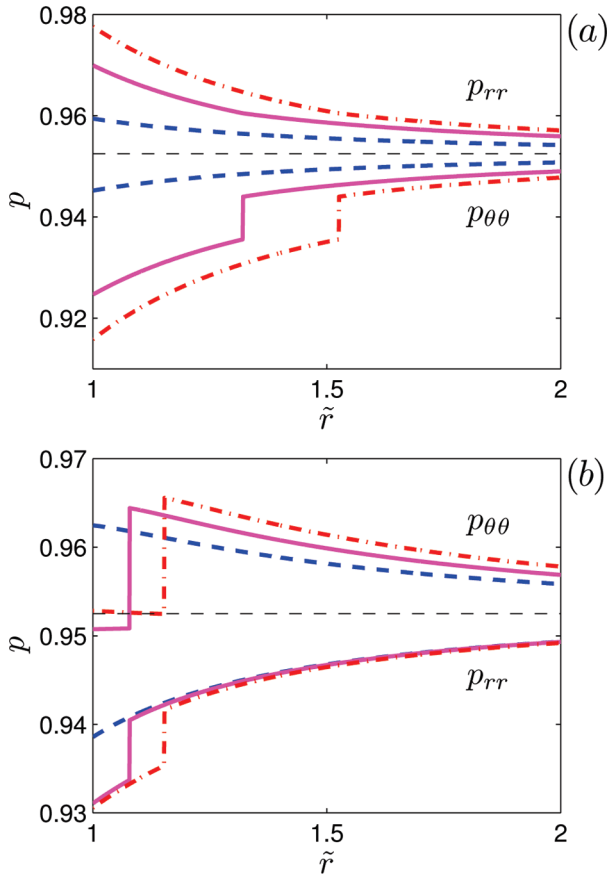

Figure 3. Radial (p_{rr}) and azimuthal ($p_{\theta\theta}$) pressure profiles corresponding to the density profiles in Figure 2. Horizontal dashed line is $p_0(\phi_0)$. In (a) the discontinuity in p_{rr} is very small.

In the wedge geometry the reduced pressure p reads

$$p = p_0 - M_w\left(\pm\tilde{\varepsilon} + \phi\frac{d\tilde{\varepsilon}}{d\phi}\right)\tilde{r}^{-2} \tag{17}$$

where p_0 is the zero-field pressure given by the equation of state. The (+) sign in eq 17 corresponds to the azimuthal component of the pressure tensor $p_{\theta\theta}$ and the (−) sign to the radial and z components $p_{rr} = p_{zz}$. The off-diagonal elements of the pressure vanish. In the charged wire the pressure is given by

$$p = p_0 - M_{sc}\left(\pm\frac{1}{\tilde{\varepsilon}} + \phi\frac{d\tilde{\varepsilon}/d\phi}{\tilde{\varepsilon}^2}\right)\tilde{r}^{-2} \tag{18}$$

where the (+) sign corresponds to p_{rr} and (−) the sign to $p_{\theta\theta} = p_{zz}$.

In Figure 3 we show the pressure curves p_{rr} and $p_{\theta\theta}$ corresponding to the density profiles in Figure 2. The pressure is discontinuous at a sharp interface. In Figure 3a the discontinuity in p_{rr} is very small. In the wedge geometry we find that $p_{\theta\theta} < p_0 < p_{rr}$ because the field is in the θ direction. In the cylindrical geometry the situation is more complex: the **r**-directed field destabilizes the interface and hence $p_{rr} < p_0$. However, in the vapor-phase $p_{\theta\theta}$ is larger than p_0, while in the liquid phase $p_{\theta\theta}$ can be larger or smaller than p_0. Note that the pressure inside the liquid droplet is smaller than in the surrounding vapor. This apparent breakdown of Laplace's formula is due to the existence of a body force of electrostatic origin.

The density difference

$$\Delta\phi = \phi_2 - \phi_1 \tag{19}$$

at the demixing interface is an important quantity. The conditions for a discontinuity from ϕ_1 to $\phi_2 > \phi_1$ at a point $\tilde{\mathbf{R}}$ in the sharp interface limit are

$$\tilde{f}'_{vdw}(\phi_1) - \frac{1}{2}\tilde{\varepsilon}'(\phi_1)\tilde{\mathbf{E}}^2(\tilde{\mathbf{R}}) - \tilde{\mu}_0 = 0 \tag{20}$$

$$\tilde{f}'_{vdw}(\phi_2) - \frac{1}{2}\tilde{\varepsilon}'(\phi_2)\tilde{\mathbf{E}}^2(\tilde{\mathbf{R}}) - \tilde{\mu}_0 = 0 \tag{21}$$

$$\tilde{f}_{vdw}(\phi_1) \mp \frac{1}{2}\tilde{\varepsilon}(\phi_1)\tilde{\mathbf{E}}^2(\tilde{\mathbf{R}}) - \tilde{\mu}_0\phi_1 = \tilde{f}_{vdw}(\phi_2) \mp \frac{1}{2}\tilde{\varepsilon}(\phi_2)\tilde{\mathbf{E}}^2(\tilde{\mathbf{R}}) - \tilde{\mu}_0\phi_2 \tag{22}$$

where the apostrophe sign indicates differentiation with respect to ϕ and $\tilde{\mathbf{E}} \equiv (P_c/\varepsilon_0)^{1/2}\mathbf{E}$ is the dimensionless electric field. The first two equations are eq 10 calculated at $\tilde{\mathbf{R}}$, and the third one is the condition that a high density is as favorable as the low density: $\tilde{\omega}(\phi_1) = \tilde{\omega}(\phi_2)$.[37] This set of equations determines ϕ_1, ϕ_2, and $\tilde{\mathbf{R}}$. The negative sign in eq 22 corresponds to constant potential and the positive sign to the constant charge case. Insertion of eqs 20 and 21 into eq 22 gives

$$\tilde{\omega}_{vdw}(\phi_1) \mp \frac{\tilde{\varepsilon}(\phi_1)}{\tilde{\varepsilon}'(\phi_1)}\tilde{\omega}'_{vdw}(\phi_1) = \tilde{\omega}_{vdw}(\phi_2) \mp \frac{\tilde{\varepsilon}(\phi_2)}{\tilde{\varepsilon}'(\phi_2)}\tilde{\omega}'_{vdw}(\phi_2) \tag{23}$$

where $\tilde{\omega}_{vdw}(\phi) = \tilde{f}_{vdw}(\phi) - \tilde{\mu}_0\phi$ is the van der Waals grand potential density.

In zero fields, eq 23 reduces to the equality $\tilde{\omega}_{vdw}(\phi_1) = \tilde{\omega}_{vdw}(\phi_2)$ and its solutions are the liquid and vapor densities $\phi_l = \phi_v$ and $\phi_2 = \phi_l$, respectively. Equation 23 shows that when phase-separation occurs, the dielectric ratio $\tilde{\varepsilon}/\tilde{\varepsilon}'$ is the significant quantity determining the densities at the interface and the location of the interface. A detailed investigation of the nonlinear equation eq 23 reveals that the dielectric ratio determines the relation between $\Delta\phi$ and the density difference at the liquid−vapor interface $\Delta\phi_b \equiv \phi_l - \phi_v$ in the absence of an electric field. At a constant potential (wedge geometry), $\tilde{\varepsilon}(\phi)$ is usually convex and $\Delta\phi > \Delta\phi_b$, whereas in the constant charge case (cylindrical system) $\Delta\phi$ can be larger or smaller than $\Delta\phi_b$.

A simple derivation of this result is possible near the critical point $(\phi_c,t_c) = (1,1)$. We employ the Landau expansion of $\tilde{f}_{vdw}$ in powers of $\phi - 1$ for t close to 1 and expand $\tilde{\varepsilon}(\phi)$ in eq 14 at $t = 1$ up to second order in $\phi - 1$

$$\tilde{\varepsilon}(\phi) = \tilde{\varepsilon}_c + \tilde{\varepsilon}'(\phi - 1) + \tilde{\varepsilon}''(\phi - 1)^2 + \ldots \tag{24}$$

Thus, eq 10 (with $m = 0$) for a constant potential can be rewritten as

$$6(t - 1)(\phi - 1) + \frac{3}{2}(\phi - 1)^3 - \tilde{\varepsilon}''(\phi - 1)\tilde{\mathbf{E}}^2(\tilde{\mathbf{R}}) - \tilde{\mu}_E = 0 \tag{25}$$

where the chemical potential $\tilde{\mu}_E$ is $\tilde{\mu}_E = \tilde{\mu} + \tilde{\varepsilon}'\tilde{\mathbf{E}}^2(\tilde{\mathbf{R}})/2$. By symmetry the densities ϕ_1 and ϕ_2 satisfy the Maxwell equal area rule for $\tilde{\mu}_E = 0$. Hence, by eq 25

$$\phi_{1,2} = 1 \mp \sqrt{4(1-t) + \frac{2\tilde{\varepsilon}''}{3}\tilde{\mathbf{E}}^2(\tilde{\mathbf{R}})} \qquad (26)$$

A similar derivation leads in the constant charge case to

$$\phi_{1,2} = 1 \mp \sqrt{4(1-t) - \frac{2}{3}\frac{\tilde{\varepsilon}'^2 - \tilde{\varepsilon}_c\tilde{\varepsilon}''}{\tilde{\varepsilon}_c^3}\tilde{\mathbf{D}}^2(\tilde{\mathbf{R}})} \qquad (27)$$

where we expanded $\tilde{\varepsilon}^{-1}$ up to second order in powers of $\phi - 1$. In the absence of the field, $\phi_{1,2} = 1 \pm \sqrt{4(1-t)}$ are the binodal densities. Since the electrostatic terms in eqs 26 and 27 have opposite signs ($\tilde{\varepsilon}'' > 0$), the difference between $\Delta\phi$ and $\Delta\phi_b$ for constant potential/charge becomes clear. The significance of this result will be understood when we discuss the vapor−liquid surface tension in section 3.3.

3.2. Stability Diagrams. In the previous section we showed density curves for a few points (ϕ_0,T,M) in the phase diagram. One can now keep M constant and calculate the stability curve $\phi_0^*(T)$ in the $\phi_0 - T$ plane. We consider only the region outside the binodal curve where the unperturbed fluid is homogeneous. Between the binodal curve and the stability curve the homogeneous fluid becomes unstable under the influence of the field and phase separation occurs, whereas outside ϕ_0^* the fluid's density varies smoothly in space.

Figure 4 shows ϕ_0^* for three materials: two are polar fluids (acetonitrile and acetone) and one nonpolar (ethane). As is seen from the solid curve (closed system) and the dash-dot curve (open system) in Figure 4a, the unstable region is slightly larger for an open system. The reason is that in a closed system material conservation dictates that a change in the liquid density is accompanied by a change in the vapor density, and this is associated with an energy penalty in f_{vdw}.

The unstable region grows with increasing value of M: compare the solid curve in Figure 4 (a) with ϕ_0^* in the inset of Figure 4 (a) where M is 100 times smaller. Even for this small value of M, the unstable region is significant near T_c.

Compared to the wedge, a larger field is required to induce phase separation in the cylindrical geometry and the unstable region is accordingly smaller. In the wedge, the unstable region is largest for acetonitrile, smaller for acetone, and very small for ethane. In contrast, in the cylindrical geometry the unstable region is largest for acetone and smaller for acetonitrile and ethane (which have regions of similar size). This qualitative difference is due to the different electrostatic term in the density equations. The wedge has a term proportional to $d\tilde{\varepsilon}/d\phi$ in eq 13. From Onsager's relation (eq 14) near ϕ_c we see that $\tilde{\varepsilon} \approx \mu_D{}^2\rho$ + constant and hence $d\tilde{\varepsilon}/d\phi \approx \mu_D{}^2$. This explains the behavior of ϕ_0^* in the wedge since μ_D is largest for acetonitrile and vanishes for ethane. To explain the behavior in the cylinder geometry we note that eq 12 has a term proportional to $g(\phi) \equiv (d\tilde{\varepsilon}/d\phi)/\tilde{\varepsilon}^2$. We plot $g(\phi)$ in Figure 5. From this figure we deduce that $g(\phi)$ and hence the field effect is largest for acetone. For acetonitrile and ethane, the average value of $g(\phi)$ is close and hence the effect is similar.

Figure 4 shows that the instability region of closed systems extends to values of ϕ_0 larger than ϕ_c, meaning that a vapor bubble can be nucleated from a homogeneous liquid. Here, the dielectrophoretic force increases the liquid density near $\tilde{R}_1$ (where the field is large) and depletes the fluid near $\tilde{R}_2$ (where the field is small). A vapor phase will be created at $\tilde{R} = \tilde{R}_2$ if the density at this region is close to the binodal density. Appearance of the phase-separation interface at $\tilde{r} = \tilde{R}_2$ requires larger voltages because the field squared at $\tilde{R}_2$ is smaller by a factor of $(\tilde{R}_2/\tilde{R}_1)^2$ compared to the field at $\tilde{R}_1$.

The stability curves in Figure 4 are piecewise continuous. They have kinks at temperatures we denote $T_{k,1}$ for $\phi_0 < \phi_c$ and

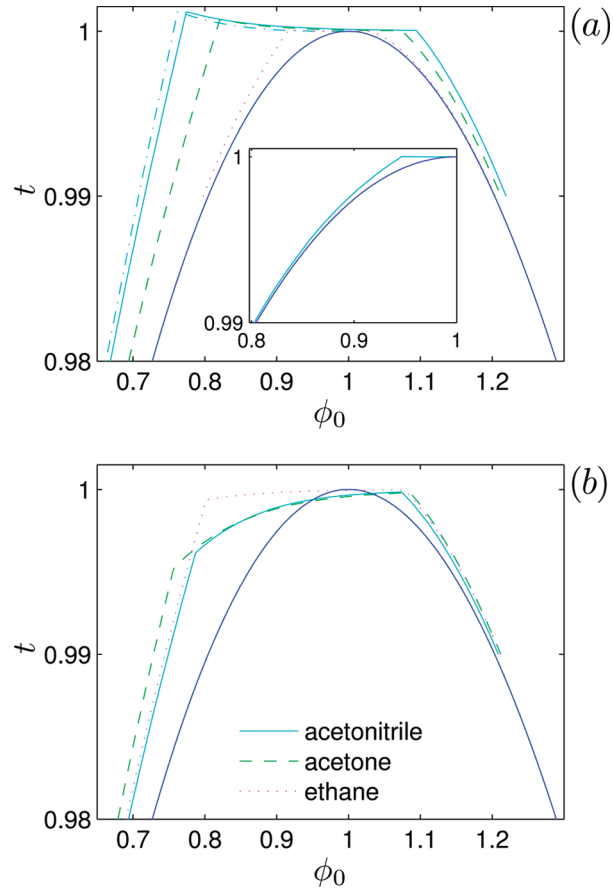

Figure 4. (a) Stability diagram for a closed and an open wedge with $M_w = 4 \times 10^{-3}$. Three materials with different dielectric properties are shown for a closed wedge: acetonitrile (solid line), acetone (dashed line), and ethane (dotted line). For an open wedge we show the stability diagram of acetonitrile (dash-dot line). (Inset) The same but with $M_w = 4 \times 10^{-5}$. The blue curve is the binodal curve $\phi_{l,v}(T)$ in the absence of field. (b) Stability diagram for concentric cylinders with $M_{sc} = 8 \times 10^{-2}$ and the same fluids as in (a). For closed systems we used $\tilde{R}_2 = 5$.

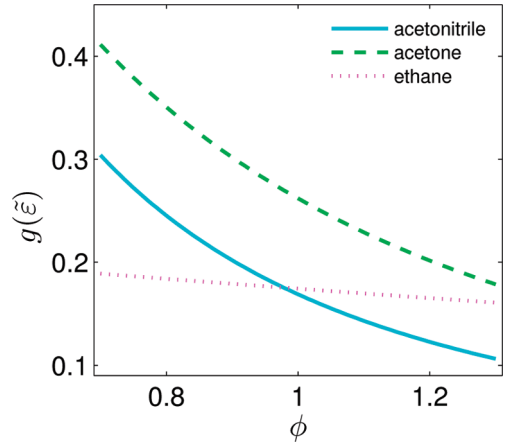

Figure 5. The function $g(\tilde{\varepsilon}) \equiv (d\tilde{\varepsilon}/d\phi)/\tilde{\varepsilon}^2$ for acetonitrile, acetone, and ethane at $t = 0.99$.

$T_{k,2}$ for $\phi_0 > \phi_c$. These kinks can be understood by looking at the second derivative $\tilde{f}'' = \partial^2\tilde{f}/\partial\phi^2$. This derivative is given by

$$\tilde{f}'' = \frac{\partial^2\tilde{f}_{vdw}}{\partial\phi^2} - M_w\frac{d^2\tilde{\varepsilon}}{d\phi^2}\tilde{r}^{-2} \quad (28)$$

for the wedge geometry. Since $\tilde{\varepsilon}(\phi)$ is a convex function, the electrostatic term in eq 28 is negative and $\tilde{f}''$ can be negative even at $T > T_c$. This means that a phase separation is possible even above T_c. For the cylinders

$$\tilde{f}'' = \frac{\partial^2\tilde{f}_{vdw}}{\partial\phi^2} + M_{sc}\frac{2(d\tilde{\varepsilon}/d\phi)^2 - \tilde{\varepsilon}(d^2\tilde{\varepsilon}/d\phi^2)}{\tilde{\varepsilon}^3}\tilde{r}^{-2} \quad (29)$$

The electrostatic term in eq 29 is positive, and hence, the unstable region is suppressed below T_c.

On the section of ϕ_0^* connecting the two kink points, phase separation occurs at a finite value of $\tilde{R}$, $\tilde{R}_1 < \tilde{R} < \tilde{R}_2$. On this "critical" line the density at $\tilde{R}$ satisfies

$$\frac{\partial^2\tilde{f}}{\partial\phi^2}(\tilde{R}) = 0, \quad \frac{\partial^3\tilde{f}}{\partial\phi^3}(\tilde{R}) = 0 \quad (30)$$

The kink points are therefore the transition points in ϕ_0^* from a first-order phase transition to a second-order phase transition. As we cross the section of ϕ_0^* between them from the stable region into the unstable region, $\Delta\phi$ increases continuously from zero. As we cross into the unstable region at the other two sections of ϕ_0^*, $\Delta\phi$ jumps abruptly from zero to a finite value.

The kink temperatures $T_{k,1}$ and $T_{k,2}$ may be found by setting in eq 30 $\tilde{R} = \tilde{R}_1$ and $\tilde{R} = \tilde{R}_2$, respectively. The expansion of $\tilde{\varepsilon}(\phi)$ (eq 24) allows us to approximate these temperatures for the wedge geometry

$$\frac{T_{k,1}}{T_c} = 1 + \frac{\tilde{\varepsilon}''M_w}{3\tilde{R}_1^2} \quad (31)$$

$$\frac{T_{k,2}}{T_c} = 1 + \frac{\tilde{\varepsilon}''M_w}{3\tilde{R}_2^2} \quad (32)$$

For acetonitrile we find $T_{k,1} - T_c \cong 0.6$ K ($M_w = 4 \times 10^{-3}$). Solving eq 30 numerically for the cylindrical case with $M_{sc} = 8 \times 10^{-2}$ we find $T_{k,1} - T_c = -2.1$ K. These estimates are 2 orders of magnitude larger than the change in T_c in uniform fields.[2,3,5]

3.3. Surface Tension. In real systems the interface between phases is not sharp but microscopically diffuse. A surface tension γ is associated with the interfacial area. In the presence of a long-range electric field, an increase of the area of the interface by A does not increase the energy by $\gamma \times A$ because displacement of the interface changes the electric field far away and leads to a volume contribution to the energy.

In order to examine the effect of the electric field on the fluid's surface tension we apply the squared gradient approximation eq 8 and solve the Euler−Lagrange equations (eqs 12 and 13) numerically for $m \neq 0$. We find that inclusion of the $(\nabla\rho)^2$ term leads to a smoothing of the density profiles on a microscopic scale but does not change the results presented thus far on the mesoscopic scale.

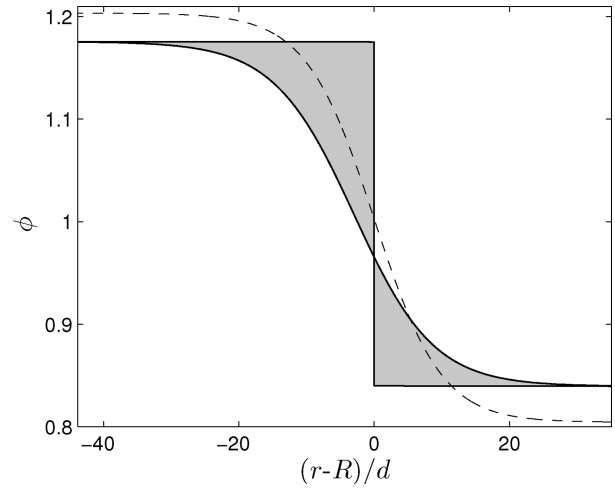

Figure 6. Zoom of the interface region of the dash-dot density profile in Figure 2b. Distance is measured in units of the molecular diameter, and the Gibbs dividing surface is taken as the origin. The shaded areas are equal. The dashed line is the zero-field vapor−liquid interface at the same temperature.

The smooth line in Figure 6 shows the interface profile $\phi^I \equiv \phi(\tilde{r};m)$, while the step curve is the density profile in the sharp interface limit $\phi^S \equiv \phi(\tilde{r};m = 0)$. The distance in this figure is measured in units of the molecular diameter. As expected, the $(\nabla\rho)^2$ is only appreciable around $\tilde{R}$ defined by eqs 20−22. It can be shown that mass conservation leads to $\tilde{R}$ being equal to the equimolar Gibbs dividing surface defined by

$$\int_{\tilde{R}_1}^{\tilde{R}}[\phi^S - \phi^I]d\tilde{r} = \int_{\tilde{R}}^{\tilde{R}_2}[\phi^I - \phi^S]d\tilde{r} \quad (33)$$

meaning that the two shaded areas in Figure 6 have equal areas.

The thermodynamic surface tension γ is the excess of the grand potential per unit area due to formation of the surface. ϕ^S is the reference profile through which we define the surface tension γ[38]

$$\begin{aligned}\frac{\gamma}{P_cR_1} &= [\tilde{\Omega}(\phi^I) - \tilde{\Omega}(\phi^S)]/A \\ &= \int_{\tilde{R}_1}^{\tilde{R}_2}\left[\frac{1}{2}\tilde{m}|\nabla\phi^I|^2 + \tilde{\omega}(\phi^I) - \tilde{\omega}(\phi^S)\right]d\tilde{r}\end{aligned} \quad (34)$$

where A is the interfacial area. The surface tension is related to density difference $\Delta\phi$ at the interface. A large value of $\Delta\phi$ results in large density gradient which increases γ. γ depends on the location of the interface $\tilde{R}$ because $\tilde{\omega}(\phi^I)$ and $\tilde{\omega}(\phi^S)$ depend on $\tilde{R}$.

We define γ_0 to be the zero-field surface tension between two coexisting phases having binodal densities at a given temperature. We find that near the critical point, the mean-field result for the surface tension of a one-component fluid[24]

$$\frac{\gamma}{P_cR_1} = \frac{1}{6}\left(\frac{\tilde{m}B}{2}\right)^{1/2}(\Delta\phi)^3 \quad (35)$$

holds for both γ and γ_0. For γ_0, eq 35 is used with $\Delta\phi_b$ instead of $\Delta\phi$. Here $B = 3/2$ is the coefficient of the $(\phi - 1)^3$ term in the Landau expansion of $\tilde{f}_{vdw}$ in powers of $\phi - 1$. In Figure 7,

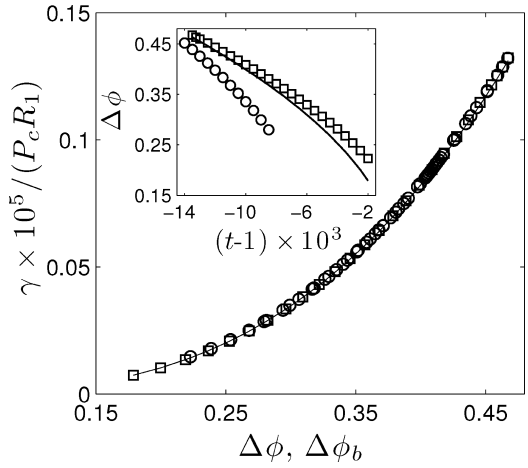

Figure 7. Surface tension as a function of the density difference at the interface. For the wedge and cylinders we plot all the data of Figure 8 (circles) vs $\Delta\phi$ and for the zero-field case at temperatures $0.868 \leq t \leq 0.993$ (squares) vs $\Delta\phi_b$. The solid line is eq 35. (Inset) Density difference as a function of temperature at $\phi_0 = 0.75$. Squares are for a wedge with $M_w = 4 \times 10^{-3}$ and circles are for a wire with $M_{sc} = 8 \times 10^{-2}$. The solid line is $\Delta\phi$ for the zero-field case, $\Delta\phi_b$, showing that $\Delta\phi > \Delta\phi_b$ for a wedge while $\Delta\phi < \Delta\phi_b$ for the cylinders.

the surface tensions γ calculated numerically using eq 34 for the wedge and cylinders and γ_0 (zero field) are shown to be consistent with eq 35.

The derivation of eq 35 shows that linear and quadratic terms in the Landau expansion of $\tilde{f}'$ in $\phi - 1$ do not contribute to γ.[24] Since the Landau expansion of the electrostatic energy (eq 25) contains terms only up to second order in $\phi - 1$, γ and γ_0 are described both by the mean-field theory in the absence of a field. Physically, eq 35 holds because of the long-range nature of the field. Since the field changes over a length scale much larger than the interface width, the field and hence the energy are nearly constant in each phase near the interface, as in the zero-field case. This is in contrast to systems where ions reside at the interface.[16,26,39] Here, the electric field changes significantly at length scales comparable to the width of the interface and eq 35 is not expected to hold.

Figure 8 is a plot of the surface tension change defined by

$$\Delta\gamma = \gamma(T, \phi_0, M) - \gamma_0(T) \tag{36}$$

In section 3.1 we have shown that $\Delta\phi < \Delta\phi_b$ for a wire while $\Delta\phi > \Delta\phi_b$ for a wedge (see inset of Figure 7), and this is the reason why $\Delta\gamma$ is negative for a wire and positive for a wedge, see Figure 8. Note that $\Delta\gamma$ is appreciable: it can be as large as 50% of γ_0, whereas in much larger uniform fields it is only a few percent of γ_0.[4]

As is seen in Figure 8, when ϕ_0 increases at constant T, $\Delta\gamma$ increases for the wire and decreases for the wedge. The reason is that in the cylindrical geometry $\Delta\phi$ and hence γ increase with ϕ_0. In the wedge $\Delta\phi$ and γ decreases with ϕ_0.

$\Delta\gamma$ depends on T via $\Delta\phi_b(T)$ as well as via $\Delta\phi(T)$. In the van der Waals theory, γ_0 decreases with T since $\Delta\phi_b \propto |t - 1|^{1/2}$ close to T_c.[25] In the presence of the field, we find that in both geometries $\Delta\phi$ and γ decrease with increasing T (see inset of Figure 7). Here, $\Delta\phi$ is excellently described near T_c by ϕ_1 and ϕ_2 given by eqs 26 and 27. The net result is a complex behavior of $\Delta\gamma$. In Figure 8 we find a concave curve with a maximum for the wedge and $\Delta\gamma$ decreases for cylinders.

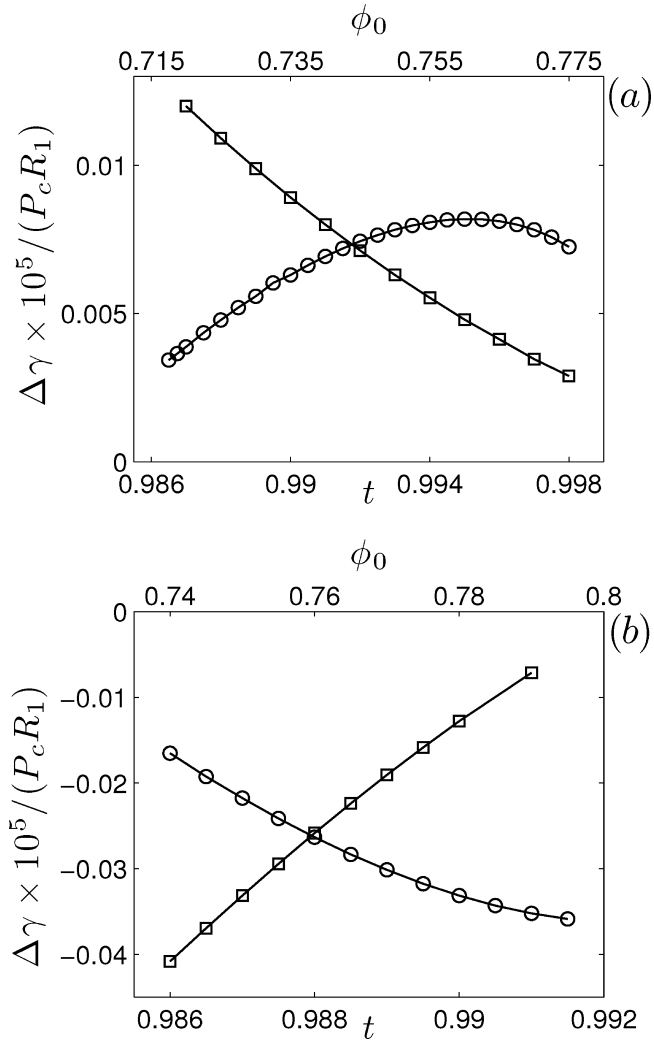

Figure 8. (a) $\Delta\gamma$ from eq 36 as a function of temperature (circles, $\phi_0 = 0.75$) and reservoir density (squares, $t = 0.99$) for an open wedge. $M_w = 4 \times 10^{-3}$ for both cases. (b) Same for a wire except that $M_{sc} = 0.08$. $\gamma_0 \times 10^5 = 0.0821 P_c R_1$ at a reduced temperature $t = 0.99$. Note that $\Delta\gamma$ is comparable to γ_0 and that $\Delta\gamma/\gamma_0$ can be as large as 0.5. We used the molecular data of acetonitrile and took $R_1 = 10$ μm, giving $P_cR_1 \approx 50$ J/m^2.

However, for a different set of parameters (T,ϕ_0,M) one may find a minimum for the cylindrical geometry.

3.4. Complex Geometries. Until now we only considered effectively one-dimensional systems. In this section we describe more complex geometries where $\mathbf{E}$ has two components: $\mathbf{E} = (E_x,E_y)$. Consider the quadrupole configuration consisting of four metal wires with alternating voltages $\pm$ V placed inside a grounded cylinder as is seen in Figure 9. As before, we find that a phase-separation transition occurs if the voltage V exceeds a critical voltage V_c. Figure 9 shows five nearly cylindrical gas bubbles nucleated from a homogeneous liquid phase when $V = 20$ V: four on the grounded surface and one at the center of the cylinder.

In general, the fluid density follows the field intensity and therefore the shapes of drops or bubbles follow the contours of $\mathbf{E}^2$, see Figure 9. Bubbles or drops appear only above a critical size, when the electrostatic gain in the bubble volume is enough to overcome the interfacial energy. Hence, when the voltage is increased from zero the four bubbles at the outer surface appear before the one at the center. As the intensity of the electric field increases, the contours of $\mathbf{E}^2$ displace and bubbles or drops grow.

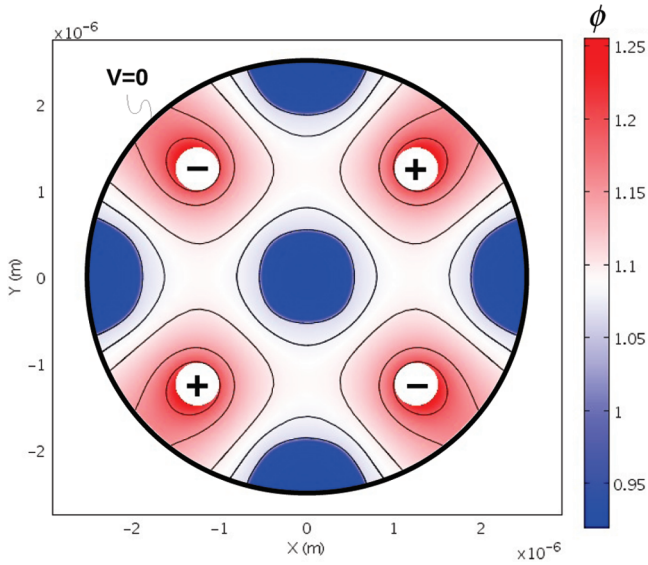

Figure 9. Nucleation of five bubbles from a homogeneous liquid in the quadrupole geometry. Large circle is a grounded external wall, while wires passing in the z direction (circles with $\pm$ signs) are charged at a potential $\pm V$. Color bar corresponds to the fluid density, and black lines are the contours of E^2. We took $t = 0.999$, $\phi_0 = 1.1$, $V = 20$ V, and the liquid parameters correspond to those of acetonitrile. Notice that the bubble at the center forms away from any confining surface.

The quadrupole configuration is an example showing that the electric field may in principle be used to create drops and bubbles of myriad shapes. By controlling the electrode configuration and the boundary conditions one can design the contours of $\mathbf{E}^2$ and thus the fluid density profile. In these complex configurations the angle between $\mathbf{E}$ and $\nabla\rho$ is not constant, and this makes it difficult to determine analytically the critical demixing charge/voltage.

4. Conclusions

We study a one-component fluid dielectric in the presence of nonuniform electric fields within the van der Waals mean-field theory. Above a critical value of the electric field, a phase-separation transition occurs and fluid drops (bubbles) nucleate from a homogeneous vapor (liquid) phase. This type of transition is general and it should occur in any bistable system with a dielectric mismatch sufficiently close to the coexistence line. We calculate the density and pressure profiles in two model geometries where the field orientation is either perpendicular or parallel to the density gradient.

The modification of the vapor−liquid coexistence by the electric field is given by stability diagrams in the temperature−density plane. The differences in the stability diagrams between closed and open systems and in the two model geometries are highlighted. These diagrams show that nonuniform fields change the transition temperature appreciably and much more than uniform fields do. The spatial dependence of the thermodynamic quantities in a nonuniform field leads to the appearance of two special points at temperatures $T_{k,1}$ and $T_{k,2}$. At the stability line connecting these points the interface appears at a finite radius $\tilde{R}$, $\tilde{R}_1 < \tilde{R} < \tilde{R}_2$.

We show that the electric field can increase or decrease the surface tension and that this change is comparable in magnitude to the zero-field surface tension. The change in surface tension is strongly dependent on temperature and average density. Although the dynamical mechanism for phase separation in nonuniform electric fields is yet to be determined, our results suggest that in a nucleation-and-growth mechanism the nucleation rates in the presence of the electric field may vary substantially as they generally depend exponentially on γ.[20]

As is shown in the quadrupole electrode array, the appearance of the phase-separation interface is not restricted to the vicinity of the confining surfaces. The quadrupole configuration also demonstrates that the electric field may be used to control and design the shape of bubbles and drops.

We suggest two experiments to test our predictions. Consider a wedge condenser immersed in a vapor near the coexistence temperature. A density gradient in the fluid implies a refractive index gradient. Beam bending and light scattering experiments[12] can probe the details of formation of a liquid drop as voltage increases. Alternatively, upon suspending a microwire in a vapor, its transverse fundamental vibration frequency is expected to changes from f_0 to f_E due to condensation of a liquid. The applied voltage is expected to be proportional to $(f_0/f_E)^2$. Room temperature experiments can be performed in substances like ethane or carbon dioxide, albeit a high-pressure cell is necessary since P_c is in the MPa range.

Acknowledgment. We gratefully acknowledge numerous discussions and correspondences with D. Andelman, C. Bechinger, M. Bier, H. Diamant, S. Dietrich, M. Kardar, A. Onuki, P. Pincus, R. Podgornik, and I. Szalai. This work was supported by the Israel Science Foundation under grant no. 11/10 and the European Research Council (ERC) "Starting Independent Researcher" grant no. 259205.

References and Notes

(1) Landau, L. D.; Lifshitz, E. M. *Elektrodinamika Sploshnykh Sred Chap. II, Sec. 18, Problem 1*; Nauka: Moscow, 1957.
(2) Szalai, I.; Chan, K.-Y.; Tang, Y. W. *Mol. Phys.* **2003**, *101*, 1819–1828.
(3) Boda, D.; Winkleman, J.; Liszi, J.; Szalai, I. *Mol. Phys.* **1996**, *87*, 601–624.
(4) Warshavsky, V. B.; Bykov, T. V.; Zeng, X. C. *J. Chem. Phys.* **2001**, *114*, 504–512.
(5) Jia, R.; Hentschke, R. *Phys. Rev. E* **2009**, *80*, 051502.
(6) Sharma, R. C. *J. Appl. Phys.* **1971**, *42*, 1234–1235.
(7) Blankenship, K. D.; DePaoli, D. W.; Hylton, J. O.; Tsouris, C. *Sep. Purif. Technol.* **1999**, *15*, 283–294.
(8) Hegseth, J.; Amara, K. *Phys. Rev. Lett.* **2004**, *93*, 057402.
(9) Debye, P.; Kleboth, K. *J. Chem. Phys.* **1965**, *42*, 3155–3162.
(10) Beaglehole, D. *J. Chem. Phys.* **1981**, *74*, 5251–5255.
(11) Orzechowski, K. *Chem. Phys.* **1999**, *240*, 275–281.
(12) Moldover, M. R.; Sengers, J. V.; Gammon, R. W.; Hocken, R. J. *Rev. Mod. Phys.* **1979**, *51*, 79–99.
(13) Tsori, Y.; Tournilhac, F.; Leibler, L. *Nature* **2004**, *430*, 544–547.
(14) Marcus, G.; Samin, S.; Tsori, Y. *J. Chem. Phys.* **2008**, *129*, 061101.
(15) Samin, S.; Tsori, Y. *J. Chem. Phys.* **2009**, *131*, 194102.
(16) Onuki, A. *J. Chem. Phys.* **2008**, *128*, 224704.
(17) Onuki, A. *Phys. Rev. E* **2006**, *73*, 021506.
(18) Ben-Yaakov, D.; Andelman, D.; Harries, D.; Podgornik, R. *J. Phys. Chem. B* **2009**, *113*, 6001–6011.
(19) Ben-Yaakov, D.; Andelman, D.; Harries, D.; Podgornik, R. *J. Phys.: Condens. Matter* **2009**, *21*, 424106.1–11.
(20) Barrat, J.-L.; Hansen, J.-P. *Basic Concepts for Simple and Complex Liquids*; Cambridge University Press: Cambridge, 2003.
(21) Heylen, A.; Postoyalko, V. *IEEE Trans. Dielectr. Electr. Insul.* **2003**, *10*, 708–714.
(22) Landau, L. D.; Lifshitz, E. M.; Pitaevskii, L. P. *Electrodynamics of Continuous Media*, 2nd ed.; Butterworth-Heinemann: Amsterdam, 1984.
(23) Onuki, A. In *Nonlinear dielectric phenomena in complex liquids*; Rzoska, S. J., Zhelezny, V., Eds.; Kluwer Academic: Dordrecht: 2004.
(24) Rowlinson, J. S.; Widom, B. *Molecular Theory of Capillarity*; Clarendon: Oxford, 1982.
(25) Onuki, A. *Phase transition dynamics*; Cambridge University Press: 2004.
(26) Onuki, A.; Kitamura, H. *J. Chem. Phys.* **2004**, *121*, 3143–3151.
(27) Tsori, Y.; Leibler, L. *Phys. Rev. E* **2005**, *71*, 032101.
(28) Morse, P. M.; Feshbach, H. *Methods of Theoretical Physics, Part I*; McGraw-Hill: New York, 1953.

(29) Lee, K. Y. C.; Klingler, J. F.; McConnell, H. M. *Science* **1994**, *263*, 655–658.

(30) Sullivan, M.; Zhao, K.; Harrison, C.; Austin, R. H.; Megens, M.; Hollingsworth, A.; Russel, W. B.; Cheng, Z.; Mason, T.; Chaikin, P. M. *J. Phys.: Condens. Matter* **2003**, *15*, S11–S18.

(31) Sullivan, M. T.; Zhao, K.; Hollingsworth, A. D.; Austin, R. H.; Russel, W. B.; Chaikin, P. M. *Phys. Rev. Lett.* **2006**, *96*, 015703.

(32) Leunissen, M. E.; Sullivan, M. T.; Chaikin, P. M.; van Blaaderen, A. *J. Chem. Phys.* **2008**, *128*, 164508.

(33) Onsager, L. *J. Am. Chem. Soc.* **1936**, *58*, 1486–1493.

(34) Chelkowski, A. *Dielectric Physics Chap. I, Sec. 17*; Elsevier Scientific Publishing Company: Amsterdam, 1980; Chapter I, Section 17.

(35) Lide, D. R., Ed.; *CRC Handbook of Chemistry and Physics*, 89th ed.; CRC Press: Boca Raton, 2008.

(36) Tsori, Y. *Rev. Mod. Phys.* **2009**, *81*, 1471.

(37) In the most general case this condition is written as $\tilde{\omega}(\phi_1) \geq \tilde{\omega}(\phi_2)$ and one has to verify that it holds first as an equality. This may not be the case if, for example, some density range becomes thermodynamically unstable due to the electric field.

(38) Sikkenk, J. H.; van Leeuwen, J. M. J. *Physica A* **1986**, *137*, 178–195.

(39) Davis, H. T.; Scriven, L. E. Stress and Structure in Fluid Interfaces. In *Advances in Chemical Physics*; Prigogine, I., S. A. R., Ed.; John Wiley & Sons: New York, 1982; Vol 49.

JP107529N